The large-scale nebular pattern of a superwind binary in an eccentric orbit

Hyosun Kim[1,5,*], Alfonso Trejo[1], Sheng-Yuan Liu[1], Raghvendra Sahai[2], Ronald E. Taam[1,3], Mark R. Morris[4], Naomi Hirano[1] & I-Ta Hsieh[1]

[1] Academia Sinica Institute of Astronomy and Astrophysics, P.O. Box 23-141, Taipei 10617, Taiwan
[2] Jet Propulsion Laboratory, California Institute of Technology MS 183-900, 4800 Oak Grove Drive Pasadena, Ca 91011, USA
[3] Department of Physics and Astronomy, Northwestern University, 2145 Sheridan Road, Evanston, IL 60208, USA
[4] University of California, Los Angeles, CA 90095-1547, USA
[5] EACOA fellow
* Corresponding author — Hyosun Kim (hkim@asiaa.sinica.edu.tw)

arXiv:1704.00449v1 [astro-ph.SR] 3 Apr 2017

Preplanetary nebulae (pPNe) and planetary nebulae (PNe) are evolved, mass-losing stellar objects that show a wide variety of morphologies. Many of these nebulae consist of outer structures that are nearly spherical (spiral/shell/arc/halo) and inner structures that are highly asymmetric (bipolar/multipolar) [1, 2]. The coexistence of such geometrically distinct structures is enigmatic because it hints at the simultaneous presence of both *wide* and *close* binary interactions, a phenomenon that has been attributed to stellar binary systems with eccentric orbits [3]. Here we report new high-resolution molecular-line observations of the circumstellar spiral-shell pattern of AFGL 3068, an asymptotic giant branch (AGB) star transitioning to the pPN phase. The observations clearly reveal that the dynamics of the mass loss is influenced by the presence of an eccentric-orbit binary. This quintessential object opens a new window on the nature of deeply embedded binary stars through the circumstellar spiral-shell patterns that reside at distances of several thousand Astronomical Units (AU) from the stars.

AFGL 3068, an extreme carbon star at the tip of the AGB evolutionary phase, is a remarkable source with the best-characterized, complete spiral pattern in its circumstellar envelope (CSE). This unambiguous spiral pattern was the first ever revealed surrounding an evolved star in a dust-scattered light image in the optical band (at $0.6\,\mu$m) of the Hubble Space Telescope (HST) [4, 5]. The striking discovery of the presence of this very well-defined pattern has prompted new research on how binarity can affect mass outflows during late stages of stellar evolution (AGB, pPN, and PN). In particular, recent theoretical investigations have shown that such patterns can naturally be explained by the orbital motion of a mass-losing star in a binary system [6–10]. In the case of AFGL 3068, there are indeed two point-like sources in its central region detected with Keck adaptive optics near-infrared imaging, revealing a projected binary separation of 109 AU [4]. Constraints on its binary parameters have been derived on the basis of these HST and Keck images, assuming a circular orbit [9]. This further indicated that the degeneracy imposed by the two-dimensional image of the three-dimensional structure can be lifted by high-resolution molecular line observations.

Our new observations of AFGL 3068 taken with the Atacama Large Millimeter/submillimeter Array (ALMA; see Methods for details on observations and data calibrations) unveil exceptionally detailed features in its CSE (Fig. 1; individual molecular lines are presented in Supplementary Figs 1–3). A

spiral pattern is definitively detected over a radius (r) of 10″, corresponding to 10,000 AU at the distance of AFGL 3068 ($\sim$3,400 light years) in the ^{12}CO $J = 2-1$ and ^{13}CO $J = 2-1$ molecular lines (see the middle panel of Fig. 1). The HC_3N $J = 24 - 23$ line best highlights the innermost winding of the spiral pattern. The emission maps integrated over the molecular lines are well correlated with the HST image, thus verifying that the circumstellar dust and molecular gas trace the same spiral feature. Remarkably, the molecular line maps reveal the presence of the innermost winding of the spiral ($r < 3''$), which was absent in the dust-scattered light image.

The observed emission pattern follows approximately a straight line when displayed in the radius (r) versus angle (ϕ) plot (Fig. 2). Such a projected shape is markedly similar to an Archimedean spiral to first-order. Hydrodynamic models show that a perfect Archimedean spiral pattern forms in the CSE surrounding a mass-losing star in a circular orbit, viewed with the orbital plane located near the plane of the sky [8].

While the molecular line emission near the systemic velocity exhibits a remarkable spiral pattern (Fig. 1, middle row panels), the emission in channels near the expansion velocity shows rather ring-like patterns (top and bottom panels). This spiral-ring bimodality has been predicted as the characteristic of binary-induced spiral-shell models having their orbits tilted with respect to the sky plane [10]. The spiral-shell models further suggest that ring-like patterns found in optical images of many AGBs, pPNe, and PNe possibly originated from binary systems, but viewed at a range of inclination angles [7–10].

The most exceptional feature of the images presented here is the previously unrecognized bifurcation in the spiral pattern (i.e., a separation and divergence of the otherwise single-stranded pattern at a given position angle). A bifurcation is visible at the second winding ($r \sim 4''$ to the North-East in the central velocity channel) and shifts toward smaller radii at larger velocity channels. A similar bifurcation structure is also found at the first winding of the spiral at $r \sim 2''$ (see Fig. 3a, dotted lines). These bifurcation features appear prominently in the angle–radius plot (Fig. 3b) as revealed by the descending trend, superimposed on the ascending trend of the main spiral pattern.

We suggest that a binary system in an eccentric orbit provides the most plausible explanation for the bifurcation seen in AFGL 3068. Following Kepler's second law, the speed of the star is fastest at the periastron, thus boosting the wind material most strongly in the direction of motion. The resulting wind gusts produced at periastron overtake the material expanding with slower speeds that was ejected throughout the orbit by spherical mass loss from the AGB star (see Supplementary Fig. 4). This leads to a spatial distribution of gas that is manifested as a local bifurcation. Fig. 3 presents a comparison between the molecular emission at the systemic velocity observed by ALMA (top) and the corresponding gas mass distribution within the same velocity range in a hydrodynamic model (bottom; see Methods for the hydrodynamic model setup). The model of a binary system in an eccentric orbit generates bifurcations that are coincident with those present in the observed images.

Bifurcations of the pattern have never appeared in previous binary models based on circular orbits. In a circular orbit model with the orbital plane inclined with respect to the plane of the sky, the spiral-shell can exhibit an undulation (with respect to the straight line characterizing an Archimedean spiral) in the angle–radius plot [10]. However, there is no inclination angle at which a bifurcation is produced.

Three-dimensional hydrodynamic simulations, assuming zero orbital eccentricity, showed that the width of the spiral pattern increases with radial distance [8]. As a result, the inner and outer edges of the thickened spiral pattern may resemble a bifurcation. The growth rate of the pattern width, however, is proportional to the ratio of the local sound speed to the wind expansion speed, which is typically less than 10% over the CSEs of AGB stars. Therefore, the separation between the inner and outer edges of the pattern would be unresolvable, as 10% of the arm-to-arm interval in AFGL 3068 is

less than 0.″3. More critically, both edges of the spiral arm should be ascending in the angle–radius plot, unlike the descending trend seen for the bifurcated features of AFGL 3068.

In another study, a periodic mass loss from a star was introduced to mimic the effect of episodic close interactions with its binary companion [11]. This model with the modulated gas densities, and hence the modulated molecular line intensities, produced very complex overlapping ring patterns rather than well-defined bifurcation features in the CSE. The dynamical influence induced by the non-circular orbital motion was not considered in that investigation.

There has been a growing consensus in recent decades that binarity is key for understanding the morphological diversities of pPNe and PNe [12,13], and considerable efforts have been made to achieve a census regarding their companion populations. Surveys based on radial velocity variation, photometric variability, and infrared excess indicate the presence of companions to the hot central stars of PNe with short periods [14–16]. The detection of long-period binaries relies mainly on direct imaging, and thus is difficult as evidenced by the low fraction of known binaries in such wide binary systems. Detection of companions to the AGB stars is severely hampered due to the high obscuration by the thick CSEs, the high brightness contrasts of the AGB stars relative to the hypothesized companions, and the stellar pulsations of the AGB stars. A limited ultraviolet imaging survey has had some success in indicating the presence of hot companions or hot accreting material induced by the companions [17]. Long-period AGB binaries are difficult to confirm with the above techniques. The spiral-shell patterns propagating through CSEs serve as indirect probes of the central binaries and therefore remedy the observational selection effect. The patterns further provide key constraints on the stellar and orbital parameters (i.e., stellar masses, orbital period, separation, inclination, and eccentricity) [10].

The central puzzle remains in the transition of outflow morphology from nearly spherically symmetric CSEs of AGB stars to highly asymmetric PNe. Interactions between *close* binaries are hypothesized to be responsible for breaking the spherical symmetry by facilitating the formation of circumstellar or circumbinary disks and thus opening the polar directions for the subsequent vigorous ejection of matter observed in many pPNe [18]. However, the typical dynamical timescales between consecutive arcs in the CSEs of the corresponding progenitors are best matched by the orbital periods of *wide* binaries [19–21]. The coexistence of such geometrically distinct structures therefore implies the simultaneous and enigmatic presence of both *wide* and *close* binary interactions. This conundrum may be solved by invoking binary systems having highly eccentric orbits. Strong binary interactions at the close periastron passages lead to a continuing decrease in the periastron separation, eventually resulting in the formation of a disk around the companion star that can launch collimated outflows and produce inner bipolar/multipolar structures.

Our results highlight the importance of theoretical investigations of binary systems having a wide range of eccentricities and orbital periods for explaining a broad variety of observational characteristics seen in objects during the AGB-PN transition. For example, in the short-period regime, an object like V Hydrae, a carbon star that is producing bullet-like mass ejections, is understood through an eccentric binary model with an orbital period of 8.5 years [22]. A very strong gravitational interaction involving an episode of strong accretion onto the companion is likely produced during the periastron passage, causing the collimated mass ejections. On the other hand, AFGL 3068 having a long period of $\sim$ 800 years does not exhibit such a polar outflow phenomenon. With an extreme eccentricity ($e = 0.8$), which is employed in the model presented in this paper, the periastron distance is still larger than 30 AU. The companion does not approach the AGB star sufficiently closely to produce the strong interaction needed for the formation of a disk powering a collimated outflow. The absence of disk formation at such binary separation is consistent with the results of hydrodynamic simulations [23]. Another carbon star, RW Leonis, has an orbital period in the intermediate range ($\sim$ 300 years) [10]. Its

rather broadened outflow and the double spiral feature in the central region are proposed as evidence for an eccentric binary [3].

AFGL 3068, exhibiting an almost perfect spiral pattern in the HST image, has been considered as a binary system in a circular orbit. However, our models for the detailed structures clearly revealed by the new ALMA observations of this source lead us, for the first time, to the conclusion that a binary system with a highly eccentric orbit is responsible for the envelope morphology. This implies that binaries in eccentric orbits for stars in the AGB, pPN, and PN phases may be ubiquitous over a large period range. Such an expectation follows from theoretical considerations as circularization of the orbit due to tidal effects is negligible in long-period systems [24]. Starting with this detailed study of AFGL 3068, it is highly desirable to determine the binary parameters of a large sample of objects. With such a statistical base in hand, one can better assess the role of binaries in these important transitional stages of stellar evolution, how the envelopes of such binaries are dynamically sculpted, and in particular, the role of highly eccentric binary orbits in producing the simultaneous presence of different nebular morphologies on a wide range of scales.

We note that indications of spiral-shell patterns have been observed in the circumstellar molecular line images of AGB stars with high sensitivity and resolution [3, 10, 11, 25–28]. Observations such as these enable detailed investigations of the entire nebular structure on spatial scales ranging from several to several thousand times the typical size of an AGB star and facilitate understandings of the morphological patterns of the AGB, pPN, and PN phases. Given early theoretical work on eccentric binary systems revealing distortions in the innermost windings of the spiral [29], the high angular resolution afforded by ALMA and the Karl G. Jansky Very Large Array, for example, is ideal for probing the orbital properties of embedded binaries, especially their eccentricities. Thus, as higher sensitivity and resolution observations of the spatio-kinematic structure through several windings of the spiral pattern are obtained for a statistical sample of sources, the mechanisms responsible for forming bipolar nebulae may be revealed.

In addition, the circumstellar spiral patterns preserve the fossil records of temporal evolution of the mass loss during the AGB phase. For R Sculptoris, a giant star with both a spiral and a thermal pulse shell, the spiral property was used as a timer for estimating the thermal pulsation period [25]. For another star, CW Leonis, its complex rose-window pattern was understood in terms of a binary system but requiring a mass loss variation [11]. The full intensity images covering all spatial scales will facilitate the examination of how binarity affects the return of stellar matter to the interstellar medium. Such an interpretation of the circumstellar patterns based on binarity and mass loss evolution may apply to other systems as well (e.g., the so-called pinwheel structure in Wolf-Rayet binaries [30]). However, details differ as the shocks in the Wolf-Rayet systems are due to colliding winds.

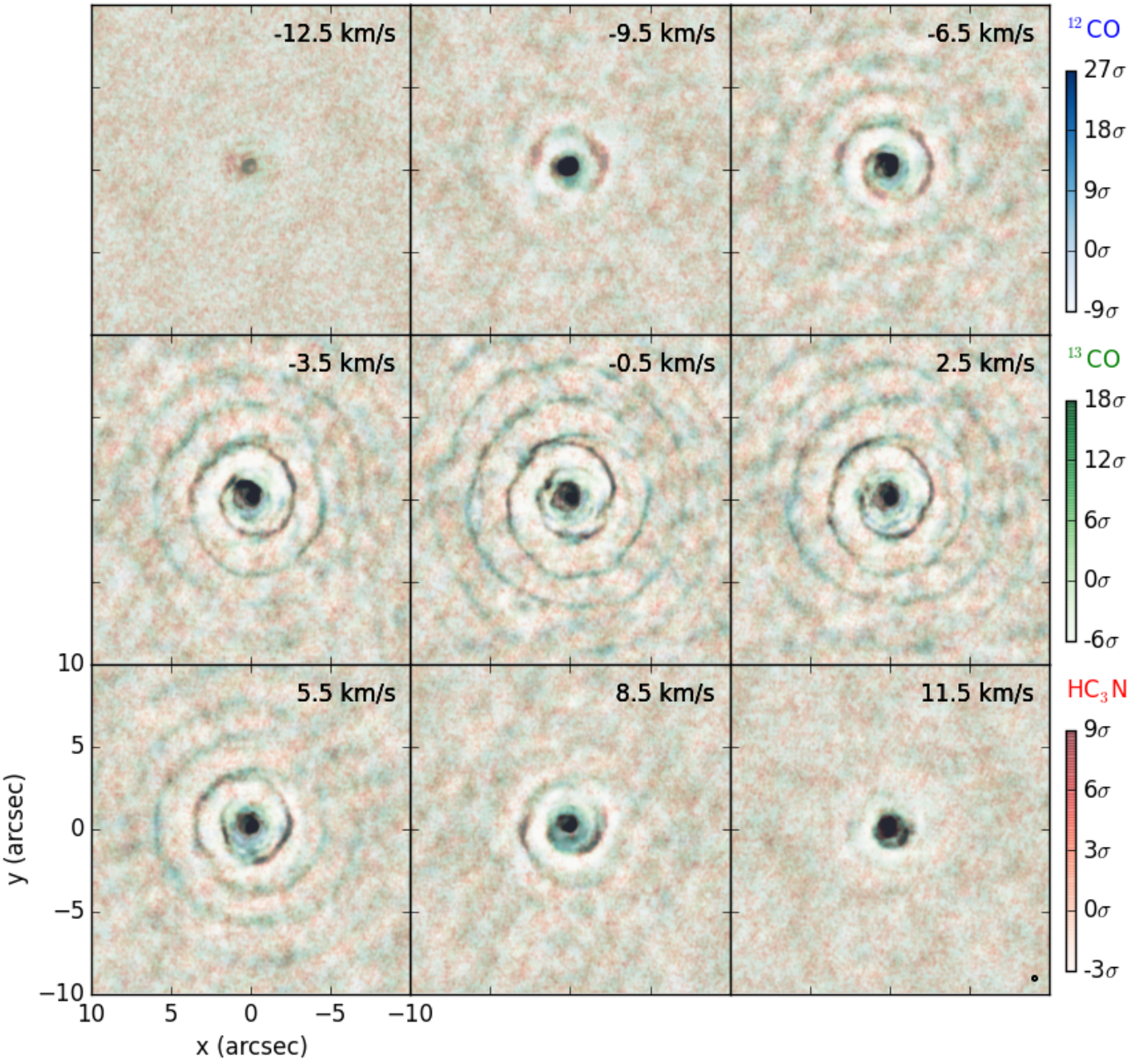

Figure 1: **ALMA velocity channel maps of AFGL 3068.** The intensities of three molecular lines ^{12}CO $J = 2-1$ (in blue), ^{13}CO $J = 2-1$ (in green), and HC_3N $J = 24-23$ (in red) are displayed in all panels, after subtraction of an extended circumstellar component. Each channel is resampled with a spectral width of $3\,\mathrm{km\,s^{-1}}$ and its velocity (relative to the systemic velocity) at the center of the channel is given at the top right side of each panel. The synthesized beam size is denoted at the bottom-right corner of the last panel. North is up, and east is to the left. Color bars indicate the intensity in units of the noise levels for the channel width of $3\,\mathrm{km\,s^{-1}}$; $\sigma = 2\,\mathrm{mJy\ beam^{-1}}$ for ^{12}CO and ^{13}CO, and $\sigma = 1\,\mathrm{mJy\ beam^{-1}}$ for HC_3N.

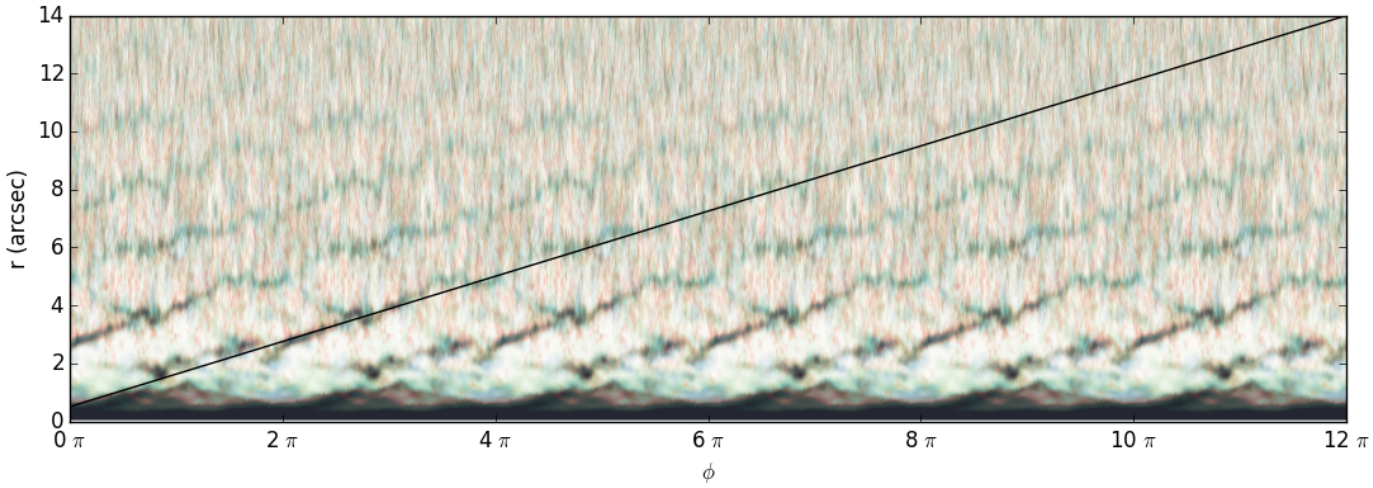

Figure 2: **Systemic velocity channel of AFGL 3068 in angle-radius plot.** Same as the middle panel of Fig. 1, but along the axes of radius from the continuum center versus angle. The angle ϕ is measured from the West ($-x$) in the counterclockwise direction. A straight line ($r_{\rm arcsec} = 0.5 + 9\,\phi/8\pi$) is inserted to guide the eyes to an Archimedean spiral, expected for a binary system in a circular orbit with the orbital plane located exactly on the plane of the sky. A reasonably good match of the observed pattern with this line indicates that an orbital period of $\sim 800\,{\rm years}\,(d/{\rm kpc})\,(V_{\rm wind}/14\,{\rm km\,s^{-1}})^{-1}$; its derivation is given in Methods. The deviation of the observed pattern from the straight line is interpreted as deviation of the binary orbit from a circle (see Fig. 3).

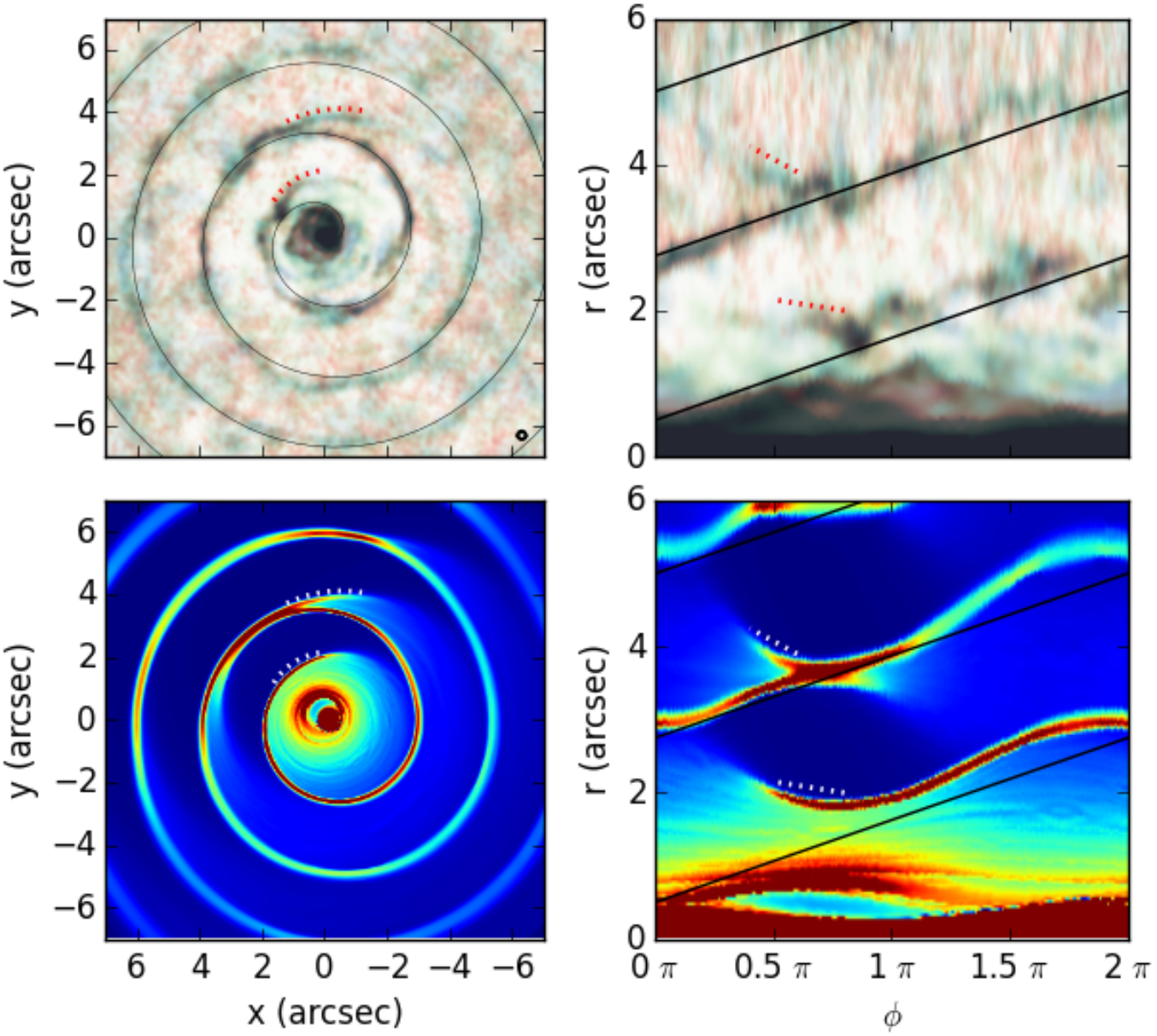

Figure 3: **Bifurcation and undulation of AFGL 3068, and an eccentric binary model.** Comparison between **(a,b)** the observed molecular line intensity at the systemic velocity and **(c,d)** the corresponding gas mass distribution within the same velocity range in a hydrodynamic model employing an eccentric binary with an eccentricity of 0.8 and an inclination angle of 50° for the orbital plane with respect to the plane of the sky. The straight line is the same as in Fig. 2. The features related to the bifurcation at two innermost windings of the spiral are marked by dotted lines (in red for the observational data, and in white for the model). The synthesized beam size of the ALMA observations is denoted as an ellipse at the bottom right side of the first panel.

Methods

ALMA observations

This paper is based on observations taken with the Atacama Large Millimeter/Submillimeter Array (ALMA) located in Chile. ALMA is currently the most sensitive and flexible millimeter/submillimeter interferometer, and it is currently in its Cycle 4 science operation. The program under project code 2013.1.00179.S, targeted at AFGL 3068 (LL Pegasi), was carried out with ALMA on August 29, August 31, and September 29 of 2015 during its Cycle 2. The integration time on AFGL 3068 was $\sim$ 1.8 hours, with the total observing time (including calibrators and overhead) $\sim$ 3.5 hours. The 5-field Nyquist-sampled mosaic observations used the 12-m array with 34 antennas on average. The correlator was configured with four spectral windows (SPWs) centered at $\sim$230.5, 232.0, 220.4, and 217.8 GHz, which fall in the ALMA Band 6 frequency coverage. The bandwidths of two SPWs for the ^{12}CO and ^{13}CO lines were 117.2 MHz, while those of the other two SPWs were individually set to 1875 MHz to maximize the sensitivity for continuum emission. The spectral resolutions of the SPWs including ^{12}CO and ^{13}CO lines were 488.281 kHz ($\sim$ 0.7 km s^{-1}), and those of the other two SPWs were 976.563 kHz ($\sim$ 1.3 km s^{-1}).

Manual calibration was performed on the data according to the standard procedures of ALMA using the Common Astronomy Software Applications (CASA) package [31]. For August 29 and 31, J2232+1143, Ceres, and J2253+1608 were used as bandpass, flux, and phase calibrators, respectively. For September 29, J2253+1608 was used as both bandpass and phase calibrators, and 3c454.3 was the flux calibrator. The use of Ceres as the flux calibrator allowed a high precision flux calibration, obtaining the calibrated flux of the phase calibrator J2253+1608 (18.45 $\pm$ 0.04 Jy at $\sim$ 230.5 GHz) with a difference between August 29 and 31 less than 1%. The calibrated flux of J2253+1608 (14.233 $\pm$ 0.004 Jy) from our data taken on September 29 is consistent with the ALMA database value to within 3% based on calibrator monitoring measurements taken on September 28.

The dataset was further self-calibrated by employing the following procedure [32]. A continuum map was first made with the line-free channels, exhibiting a compact source with a signal to noise ratio greater than 300. Two cycles of self-calibration against the continuum image were then applied to derive new phase and phase-amplitude gains. We achieved an improvement in noise level by 20%, obtaining a final r.m.s. noise of 0.2 mJy per beam in the continuum map. The synthesized beam was $0\farcs35 \times 0\farcs34$ with a robust weighting of 0.5.

The resulting calibration gains from self-calibration were applied to the line data for further imaging. We defined individual cleaning boxes on a channel by channel basis in the CLEAN task to properly account for the complex emission region. The resulting synthesized beam sizes for all molecular line images are about $0\farcs26 \times 0\farcs23$ with a robust weighting of 0.5.

Supplementary Figs 1–3 present the channel maps and angle–radius plots of ^{12}CO $J = 2-1$, ^{13}CO $J = 2-1$, and HC_3N $J = 24-23$ obtained by the ALMA observations.

Orbital period from an Archimedean spiral in a circular orbit approximation

The orbital period of a binary system is simply a function of total mass and the summation of semi-major axes of binary orbits (Kepler's third law). Therefore, its estimate in a circular orbit approximation is valid for eccentric orbit cases.

The spiral pattern in the CSE of mass-losing star forms at the location of mass ejection (i.e., $r = r_{\rm orb}$) with the balance between the radial velocity of the wind (i.e., $V_{\rm wind}$) and the tangential

velocity dragging the wind gusts to the direction of orbit (i.e., $V_{\rm orb}$). This statement corresponds to the following equation:

$$\frac{1}{r_{\rm orb}}\frac{{\rm d}r}{{\rm d}\phi} = \frac{V_{\rm wind}}{V_{\rm orb}} \tag{1}$$

Assuming a circular orbit and a constant inherent speed of the wind, it yields an Archimedean spiral, $r = A + B\,\phi$, where A and B are constant values. The A parameter indicates the standoff distance of the spiral or alternatively provides the position angle of the starting point of the spiral, which is in general difficult to identify because of complexity in the innermost region of the CSE due to a combination of small-scale anisotropy of the mass loss, molecular chemistry and insufficient sensitivity. The B parameter can be easily measured from the global slope of the observed emission pattern in the angle–radius plot, assuming a perfect Archimedean spiral. For instance, a slope ${\rm d}r/{\rm d}\phi = 9''/8\pi$ characterizes the spiral pattern of AFGL 3068 observed by ALMA to first order (as seen in Fig. 2). This slope gives a rough estimate for the orbital period of AFGL 3068, $T_{\rm orb} \sim 800\,{\rm years}\,(d/{\rm kpc})\,(V_{\rm wind}/14\,{\rm km\,s^{-1}})^{-1}$, which is derived straightforward from the definitions of orbital period $T_{\rm orb} = 2\pi r_{\rm orb}/V_{\rm orb}$ and a length unit, parsec (pc), $d/{\rm pc} = {\rm arcsec/AU}$, where d is the distance to the astronomical object.

Geometrical model for the bifurcation appearing in an eccentric binary

Supplementary Fig. 4 illustrates how the bifurcation feature observed along the circumstellar spiral pattern of AFGL 3068 forms in an eccentric binary. The net velocity of the mass-losing AGB stellar envelope is the vector sum of the inherent wind velocity (measured in the inertial frame of the AGB star) and the orbital velocity of the star. The wind speed measured from an observer therefore is fastest in the direction of motion of the orbit and slowest in the opposite direction. In a circular orbit case, such a wind ejection trend does not change along the orbital passage and results in an Archimedean spiral pattern. In an eccentric orbit, however, the orbital speed changes along the orbit with its maximum at the periastron. To better visualize this effect in Supplementary Fig. 4, we use circular rings to indicate the locations of wind gusts ejected from the AGB star at different passages through the orbit revolution. The wind gusts ejected at the periastron in the direction of motion plunge through the edge of the pattern formed in an earlier orbital cycle. Such overlap of two structures appears as a bifurcation, repeating every cycle, and serving as distinctive characteristics of eccentric orbits.

Hydrodynamic model

The observed spiral pattern in the CSE of a mass-losing star in a given eccentric binary model depends on eight key parameters. Among these, five parameters (masses of two individual stars, separation, inclination angle, and position angle of the current location of the mass-losing star) have been investigated in a parameter space analysis for circular binary models [9]. An eccentric binary model requires three additional key parameters (eccentricity, position angle of the periastron, and position angle of the node of the orbit).

In this paper, we adopt the stellar masses and their mean separation derived from a parameter space analysis under a circular orbit assumption [9] and introduce an orbital eccentricity as an extra parameter. Hence, the binary system that we employ for a hydrodynamic simulation consists of a mass-losing star and its companion with the masses of $3.5M_{\odot}$ and $3.1M_{\odot}$, respectively, a mean orbital separation of 166 AU, and an eccentricity $e = 0.8$. The wind is quickly accelerated to reach $14\,{\rm km\,s^{-1}}$ well within the region of our interest, therefore the modulation in the result is certainly due to the orbital motion. The hydrodynamic simulation is performed using the FLASH4.3 code with an adaptive mesh refinement [33] based on a piecewise parabolic method [34].

To reproduce the projected view of observed pattern, we orient the modeled density cube with four angular parameters described above (one inclination angle measured from the plane of the sky, and three position angles on the plane of the sky) based on alignment of bifurcations, elongation of spiral, undulation features in several channels, etc. In particular, the orbit in the model displayed in this paper is inclined by 50° from the plane of the sky, producing an additional undulation atop the undulation due to the eccentric orbit. The mass-losing star is located at 72° ahead of the periastron in the clockwise direction in the orbital plane. After applying the inclination, the density cube is rotated by 130° in the counterclockwise direction. The periastron, set to be on the line of nodes, is therefore located along the position angle of 40° (measured from North to the East in the plane of the sky) in Fig. 3.

The total stellar mass and mean separation (semi-major axis of the stars) would not change significantly with the inclusion of orbital eccentricity, because these two parameters are tightly linked to the orbital period, which is measured from the arm-to-arm intervals. The uncertainty for the mass is larger than that of the semi-major axis (Kepler's law). The orbital eccentricity and inclination determine the degree of undulation in the angle-radius plot, while the three position-angle parameters determine the alignment of bifurcation features, the variation of undulation amplitude within each winding, the elongation direction of the overall spiral pattern, and some details such as the variation of arm-to-arm separation as a function of position angle.

We focus on the unique characteristics of eccentric binaries, revealed by the ALMA observation in this paper, from an insightful comparison of the pattern produced by a binary in an eccentric orbit with the corresponding circular orbit case studied earlier [9]. The bifurcation feature becomes distinguishable with an eccentricity $\gtrsim 0.5$. The angle between the two branches indicates that the eccentricity is significantly larger than 0.5 with a good match to the $e \sim 0.8$ model. The location of the outer branch is mainly determined by the eccentricity, while the location of the inner branch highly depends on the inclination angle. The overall undulation seen in the angle–radius plot results from the combined effect of the eccentricity and inclination angle of the orbit, with a greater sensitivity to the eccentricity. We defer a parameter study for a thorough modeling to a future investigation.

References

[1] Balick, B. & Frank, A. Shapes and Shaping of Planetary Nebulae. *Annu. Rev. Astron. Astrophys.* **40,** 439–486 (2002).

[2] Sahai, R., Morris, M. R. & Villar, G. G. Young Planetary Nebulae: Hubble Space Telescope Imaging and a New Morphological Classification System. *Astron. J.* **141,** 134 (2011).

[3] Kim, H. et al. High-resolution CO Observation of the Carbon Star CIT 6 Revealing the Spiral Structure and a Nascent Bipolar Outflow. *Astrophys. J.* **814,** 61 (2015).

[4] Morris, M. et al. A Binary-Induced Pinwheel Outflow from the Extreme Carbon Star, AFGL 3068. In *Planetary Nebulae in our Galaxy and Beyond* (eds Barlow, M. J. & Méndez, R. H.) 469–470 (*Proceeding of the International Astronomical Union Symposium 234*, 2006).

[5] Mauron, N. & Huggins, P. J. Imaging the circumstellar envelopes of AGB stars. *Astron. Astrophys.* **452,** 257–268 (2006).

[6] Soker, N. Influences of Wide Binaries on the Structures of Planetary Nebulae. *Mon. Not. R. Astron. Soc.* **270,** 774–780 (1994).

[7] Mastrodemos, N. & Morris, M. Bipolar Pre-Planetary Nebulae: Hydrodynamics of Dusty Winds in Binary Systems. II. Morphology of the Circumstellar Envelopes. *Astrophys. J.* **523,** 357–380 (1999).

[8] Kim, H. & Taam, R. E. Wide Binary Effects on Asymmetries in Asymptotic Giant Branch Circumstellar Envelopes. *Astrophys. J.* **759,** 59 (2012).

[9] Kim, H. & Taam, R. E. A New Method of Determining the Characteristics of Evolved Binary Systems Revealed in the Observed Circumstellar Patterns: Application to AFGL 3068. *Astrophys. J. Lett.* **759,** L22 (2012).

[10] Kim, H., Hsieh, I.-T., Liu, S.-Y. & Taam, R. E. Evidence of a Binary-induced Spiral from an Incomplete Ring Pattern of CIT 6. *Astrophys. J.* **776,** 86 (2013).

[11] Cernicharo, J., Marcelino, N., Agúndez, M. & Guélin, M. Molecular shells in IRC+10216: tracing the mass loss history. *Astron. Astrophys.* **575,** A91 (2015).

[12] Soker, N. Shaping Planetary Nebulae and Related Objects. In *Asymmetrical Planetary Nebulae III: Winds, Structure and the Thunderbird Vol. 313* (eds Meixner, M., Kastner, J. H., Balick, B. & Soker, N.) 562–568 (*Astronomical Society of the Pacific Conference Series*, 2004).

[13] Soker, N. Why Magnetic Fields Cannot Be the Main Agent Shaping Planetary Nebulae. *Publ. Astron. Soc. Pacif.* **118,** 260–269 (2006).

[14] Bond, H. E. Binarity of Central Stars of Planetary Nebulae. In *Asymmetrical Planetary Nebulae II: From Origins to Microstructures Vol. 199* (eds Kastner, J. H., Soker, N. & Rappaport, S.) 115–123 (*Astronomical Society of the Pacific Conference Series*, 2000).

[15] Miszalski, B., Acker, A., Moffat, A. F. J., Parker, Q. A. & Udalski, A. Binary planetary nebulae nuclei towards the Galactic bulge. I. Sample discovery, period distribution, and binary fraction. *Astron. Astrophys.* **496,** 813–825 (2009).

[16] Douchin, D. et al. The binary fraction of planetary nebula central stars - II. A larger sample and improved technique for the infrared excess search. *Mon. Not. R. Astron. Soc.* **448,** 3132–3155 (2015)

[17] Sahai, R., Findeisen, K., Gil de Paz, A. & Sánchez Contreras, C. Binarity in Cool Asymptotic Giant Branch Stars: A GALEX Search for Ultraviolet Excesses. *Astrophys. J.* **689,** 1274-1278 (2008).

[18] Morris, M. Models for the structure and origin of bipolar nebulae. *Astrophys. J.* **249,** 572-585 (1981).

[19] Su, K. Y. L. Concentric Semi-Circular Rings/Arcs. In *Asymmetrical Planetary Nebulae III: Winds, Structure and the Thunderbird Vol. 313* (eds Meixner, M., Kastner, J. H., Balick, B. & Soker, N.) 247–253 (*Astronomical Society of the Pacific Conference Series*, 2004).

[20] Corradi, R. L. M., Sánchez-Blázquez, P., Mellema, G., Giammanco, C. & Schwarz, H. E. Rings in the haloes of planetary nebulae. *Astron. Astrophys.* **417,** 637–646 (2004).

[21] Ramos-Larios, G. et al. Rings and arcs around evolved stars – I. Fingerprints of the last gasps in the formation process of planetary nebulae. *Mon. Not. R. Astron. Soc.* **462,** 610–635 (2016).

[22] Sahai, R., Scibelli, S. & Morris, M. R. High-speed Bullet Ejections during the AGB-to-Planetary Nebula Transition: HST Observations of the Carbon Star, V Hydrae. *Astrophys. J.* **827,** 92 (2016).

[23] Huarte-Espinosa, M., Carroll-Nellenback, J., Nordhaus, J., Frank, A. & Blackman, E. G. The formation and evolution of wind-capture discs in binary systems. *Mon. Not. R. Astron. Soc.* **433,** 295-306 (2013).

[24] Verbunt, F. & Phinney, E. S. Tidal circularization and the eccentricity of binaries containing giant stars. *Astron. Astrophys.* **296,** 709–721 (1995).

[25] Maercker, M. et al. Unexpectedly large mass loss during the thermal pulse cycle of the red giant star R Sculptoris. *Nature* **490,** 232–234 (2012).

[26] Claussen, M. J. et al. A Pilot Imaging Line Survey of RW LMi and IK Tau Using the Expanded Very Large Array. *Astrophys. J. Lett.* **739,** L5 (2011).

[27] Ramstedt, S. et al. The wonderful complexity of the Mira AB system. *Astron. Astrophys.* **570,** L14 (2014).

[28] Decin, L. et al. ALMA data suggest the presence of spiral structure in the inner wind of CW Leonis. *Astron. Astrophys.* **574,** A5 (2015).

[29] Raga, A. C., Cantó, J., Esquivel, A., Huggins, P. J. & Mauron, N. Jets and winds from binary stars. In *Asymmetric Planetary Nebulae V* (eds Zijlstra, A. A., Lykou, F., McDonald, I. & Lagadec, E.) 185–191 (*Jodrell Bank Centre for Astrophysics*, 2011).

[30] Tuthill, P. G., Monnier, J. D. & Danchi, W. C. A dusty pinwheel nebula around the massive star WR104. *Nature* **398,** 487–489 (1999).

[31] McMullin, J. P., Waters, B., Schiebel, D., Young, W. & Golap, K. CASA Architecture and Application. In *Astronomical Data Analysis Software and Systems XVI Vol. 376* (eds Shaw, R. A., Hill, F. & Bell, D. J.) 127–130 (*Astronomical Society of the Pacific Conference Series*, 2007).

[32] Pearson, T. J. & Readhead, A. C. S. Image Formation by Self-Calibration in Radio Astronomy. *Annu. Rev. Astron. Astrophys.* **22,** 97–130 (1984).

[33] Fryxell, B. et al. FLASH: An Adaptive Mesh Hydrodynamics Code for Modeling Astrophysical Thermonuclear Flashes. *Astrophys. J. Suppl. Ser.* **131,** 273–334 (2000).

[34] Colella, P. & Woodward, P. R. The Piecewise Parabolic Method (PPM) for Gas-Dynamical Simulations. *J. Comput. Phys.* **54,** 174–201 (1984).

Acknowledgments
This paper makes use of the following ALMA data: ADS/JAO.ALMA#2013.1.00179.S. ALMA is a partnership of ESO (representing its member states), NSF (USA) and NINS (Japan), together with NRC (Canada), NSC and ASIAA (Taiwan), and KASI (Republic of Korea), in cooperation with the Republic of Chile. The Joint ALMA Observatory is operated by ESO, AUI/NRAO and NAOJ. H.K. acknowledges support through East Asian Core Observatories Association (EACOA) Fellowship, and thanks F. Kemper for encouraging the project and reviewing an early version of manuscript. R.S.'s contribution to the research described here was carried out at the Jet Propulsion Laboratory, California

Institute of Technology, under a contract with NASA, with financial support in part from NASA/STScI HST award (GO 11676.02).

Author contributions

H.K. planned the project, prepared and submitted the proposal, and wrote the manuscript. A.T. was involved in observation preparation, data reduction and analysis, and commented on the manuscript. S.-Y.L. was involved in project planning, data interpretation, and manuscript preparation. R.S., R.E.T., M.M. and N.H. were involved in the science discussion as well as writing the proposal and manuscript. I.-T.H. did the radiative transfer modeling in the proposal preparation that generated the data for this study.

Data availability

The data that support the plots within this paper and other findings of this study are available from the corresponding author upon reasonable request.

Additional information

Correspondence and requests for materials should be addressed to Hyosun Kim (hkim@asiaa.sinica.edu.tw).

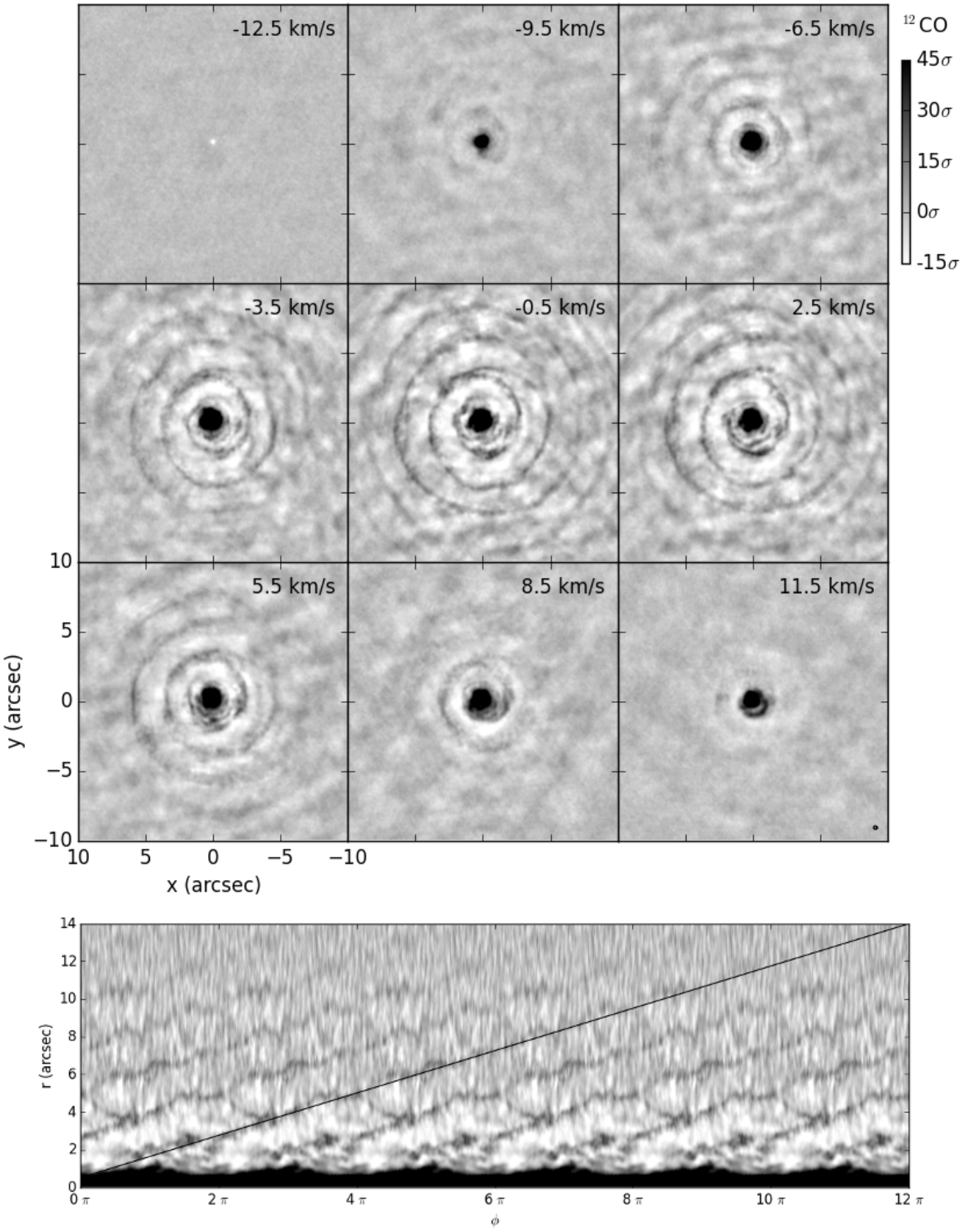

Supplementary Figure 1: **^{12}CO $J = 2 - 1$ of AFGL 3068.** The channel map (top) and angle–radius plot (bottom) of ^{12}CO molecular line emission. See Figs 1 and 2 captions for details.

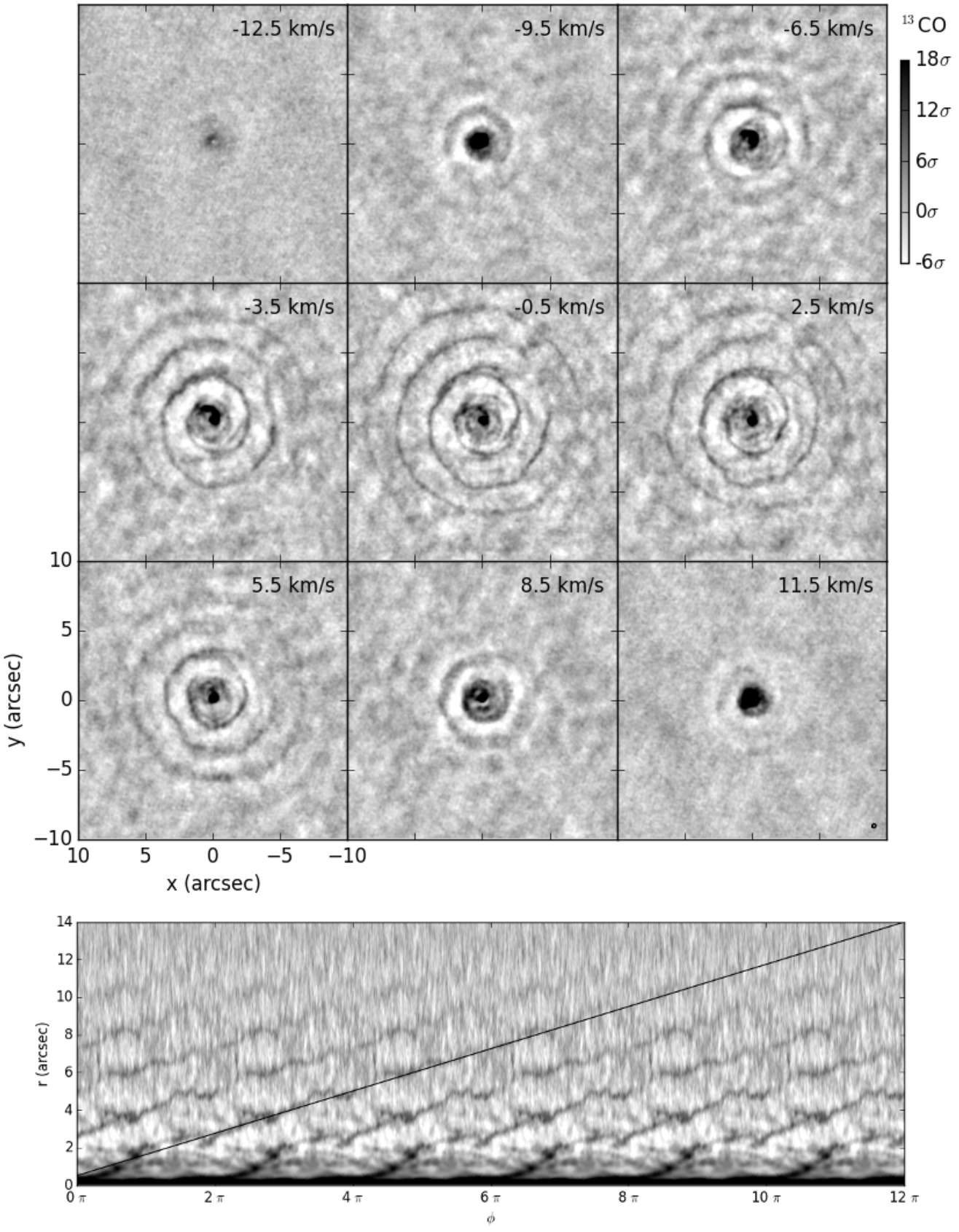

Supplementary Figure 2: **^{13}CO $J = 2 - 1$ of AFGL 3068.** The channel map (top) and angle–radius plot (bottom) of ^{13}CO molecular line emission. See Figs 1 and 2 captions for details.

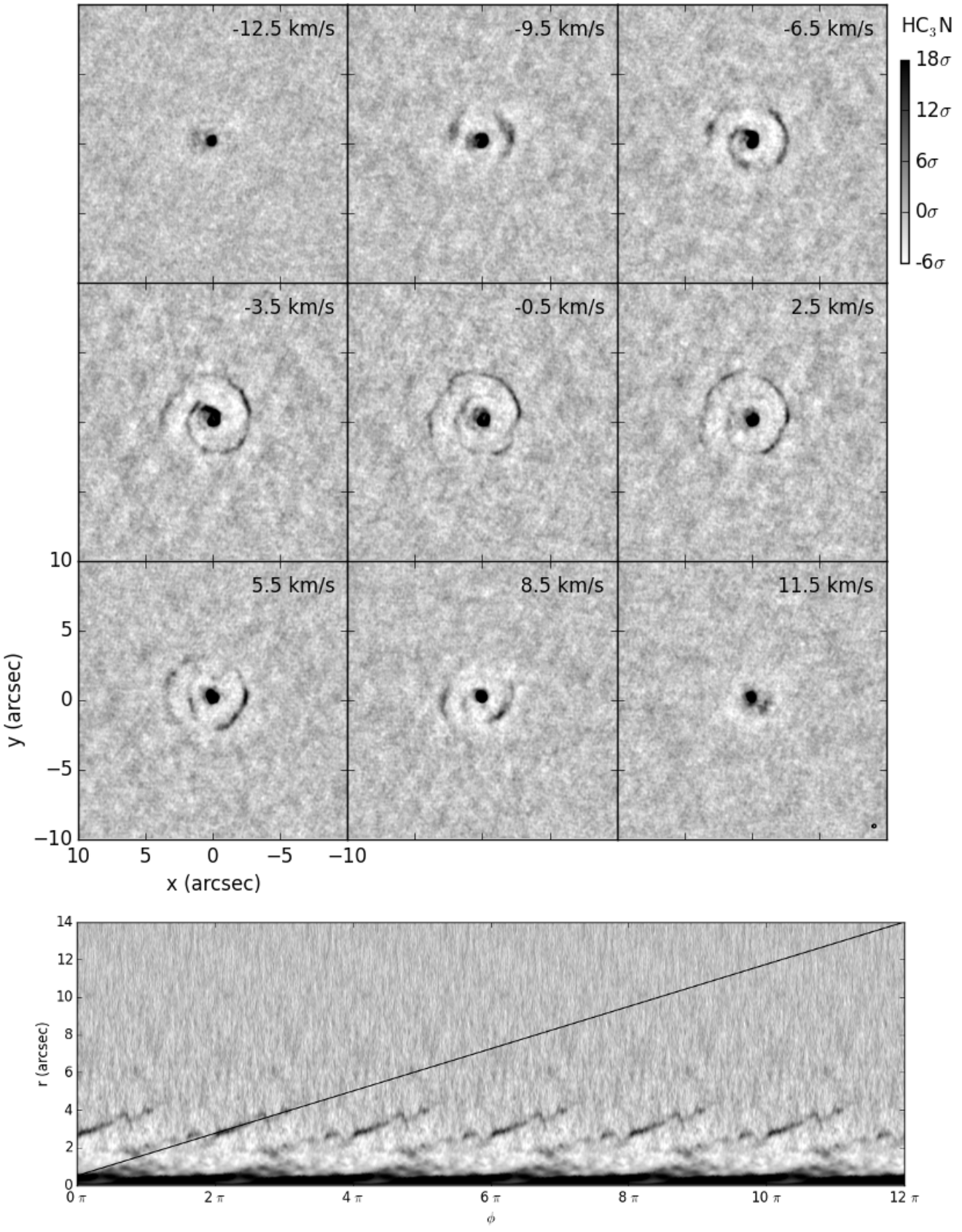

Supplementary Figure 3: **HC_3N $J = 24 - 23$ of AFGL 3068.** The channel map (top) and angle–radius plot (bottom) of HC_3N molecular line emission. See Figs 1 and 2 captions for details.

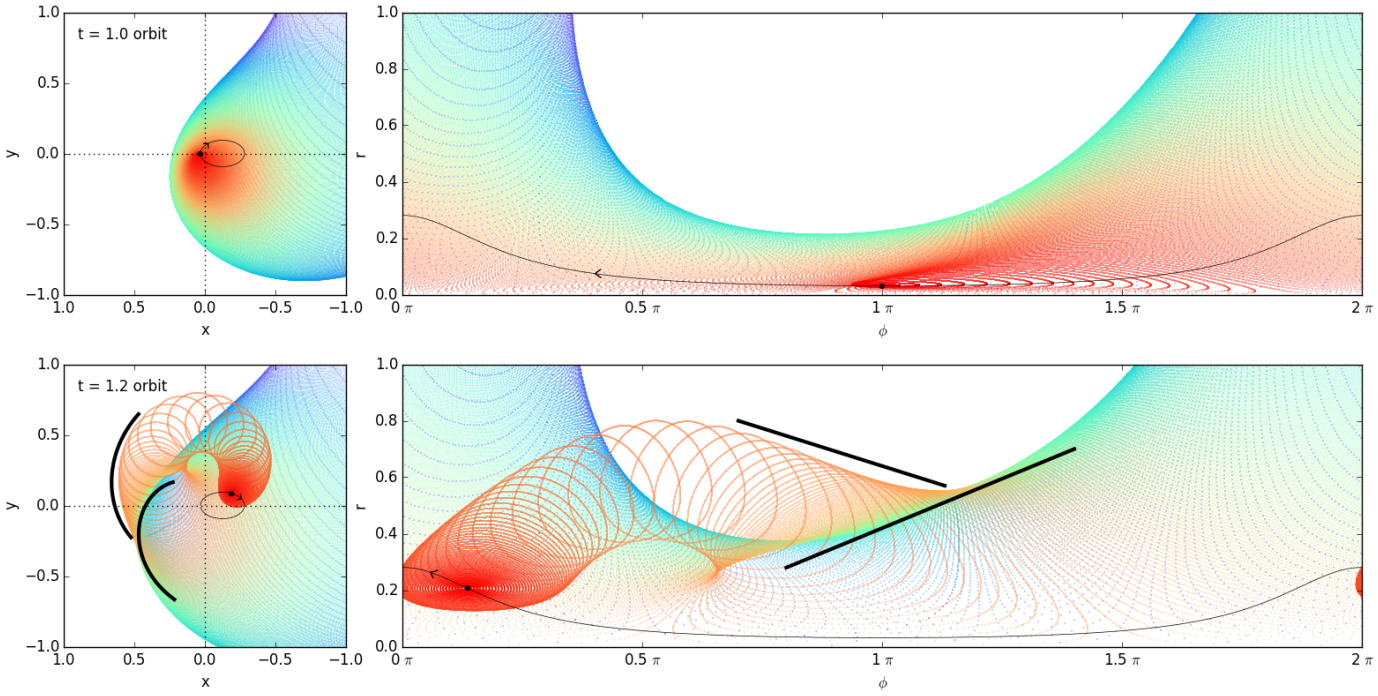

Supplementary Figure 4: **Formation of a bifurcation in an eccentric binary.** A geometrical model illustrating the distributions of wind material from a mass-losing star in the x–y plane (left) and ϕ–r plane (right) after 1 orbit (top) and 1.2 orbits (bottom) starting from the periastron of its orbit in the clockwise direction (marked by arrows). The origin of coordinates at left is at a focus of the ellipse (thin line) representing the relative location of the mass-losing star (eccentricity of 0.8). The faster wind in the forward direction of motion at the periastron overtakes the material distributed during the earlier orbit, displaying the bifurcation. Thick lines trace the feature of interest. Red to blue colors represent the ejection time sequence of wind gusts from recent to the past.

Supplementary Video 1: **Visualizing the ALMA image cube of AFGL 3068.** Each frame of the video shows the composite image of ^{12}CO $J = 2 - 1$, ^{13}CO $J = 2 - 1$ and HC_3N $J = 24 - 23$ emission for a different line-of-sight velocity. This velocity, relative to the systemic velocity, advances by $1\,\mathrm{km\,s^{-1}}$ per frame, and is given at the top-right corner. The presented field area is $10'' \times 10''$. North is up and east is to the left. (Video available from Nature Astronomy website.)